Nano Res (2009) 2: 678–687
DOI 10.1007/s12274-009-9071-2
Research Article

Thin Films of Ruthenium Phthalocyanine Complexes

Tristan Rawling, Christine E. Austin, Dominic Hare, Philip A. Doble, Hadi M. Zareie, and Andrew M. McDonagh (✉)

Institute for Nanoscale Technology, University of Technology Sydney, Sydney, NSW 2007, Australia

Received: 11 May 2009 / Revised: 4 June 2009 / Accepted: 8 July 2009

ABSTRACT

Four new ruthenium phthalocyanine complexes bearing axial ligands with thioacetate groups that facilitate thin film formation on gold surfaces are presented. Scanning tunnelling microscopy (STM) images and surface coverage data obtained by solution inductively coupled plasma mass spectrometry (ICP-MS) experiments show that peripheral and axial ligand substituents on the complexes have a significant effect on their surface coverage. A laser ablation ICP-MS technique that provides information about thin films across macro-sized areas is described here for the first time. Using the technique, the maximum surface coverage of a ruthenium phthalocyanine complex was found to occur within one minute of gold substrate immersion in the complex-containing solution.

KEYWORDS

Ruthenium; phthalocyanine; gold; surface; laser ablation

Thin films and monolayers of molecules adsorbed to surfaces have generated sustained interest due to applications in fields such as molecular and biomolecular recognition [1], corrosion protection [2], and patterning [3]. Alkanethiols are the most studied class of compounds for thin films on gold as they readily bind to the surface and the molecules may form ordered surface structures [4]. There are, however, far fewer examples of monolayers and thin films containing transition metal complexes and only a few examples of ruthenium phthalocyanine (PcRu) complexes bound to surfaces [5–10]. This class of complex offers interesting electronic and optical properties that may be utilized in a variety of applications [5, 11]. Four new complexes (Fig. 1) are presented here that bear a functionalized pyridine axial ligand through which the complexes can bind to gold.

Any development of thin film-based technology

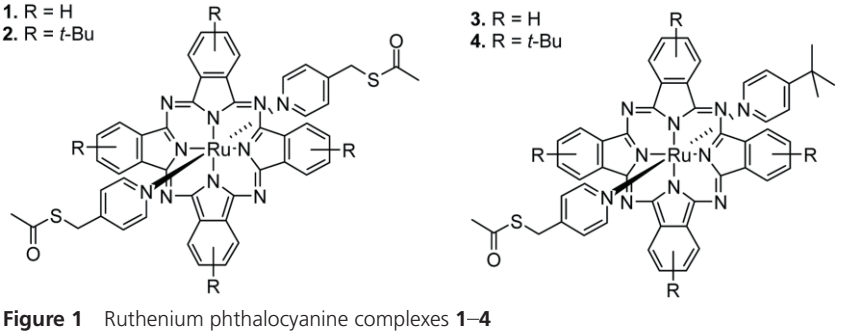

Figure 1 Ruthenium phthalocyanine complexes **1**–**4**

Address correspondence to Andrew.McDonagh@uts.edu.au

using molecules is heavily reliant upon an ability to accurately analyze and characterize the molecular films. There are numerous analytical tools [12] available to the researcher, including electronic (e.g., X-ray photoemission spectroscopy), structural (e.g., infrared spectroscopy, X-ray diffraction), and microscopic (e.g., scanned probe microscopy) techniques. Here we report for the first time a new method for the analysis of thin films containing the transition metal ruthenium by laser ablation inductively coupled plasma mass spectrometry (LA-ICP-MS). LA-ICP-MS is a relatively new technique that is used for the analysis of solid samples. The sample material is vaporized in a focused laser beam and transported with argon gas into the inductively coupled plasma ion source of an ICP-MS. The technique offers several advantages including little or no sample preparation and no solvent interferences, and importantly is able to give information about spatial distributions of elemental profiles [13]. This technique, coupled with scanning tunneling microscopy (STM) and a solution-phase ICP-MS technique allows for a detailed investigation of the coverage of surface-bound molecules. In general, mass spectrometry techniques offer exciting new possibilities in the analysis of surface-bound molecules [14]. Of relevance to the current work, ICP-MS has been utilized in the characterization of thin films of antimony on gold [15] and silicon [16] where the entire thin film was desorbed from the substrate and the resultant solution analyzed to obtain the number of atoms in the film. This solution-based technique is extremely sensitive although it does not yield any information about spatial features of the thin film being analyzed.

1. Results and discussion

1.1 Synthesis and characterization

The synthesis of the four new PcRu complexes is shown in Scheme 1. These complexes were chosen for investigation because, (1) as shown below, ruthenium is a sensitive probe for ICP-MS, (2) the Pc ligand strongly binds the metal ensuring the probe metal atom remains coordinated during thin film formation, and (3) the complex bearing thioester groups that facilitate binding to gold surfaces is readily synthetically accessible. The new complexes **1**–**4** were synthesized by substitution of the axial benzonitrile ligands of $[PcRu(PhCN)_2]$ or $[\{(t\text{-}Bu)_4Pc\}Ru(PhCN)_2]$ with functionalized pyridine ligands (Scheme 1). The pyridine ligands bear thioester groups that enable the complex to bind to gold surfaces after hydrolysis of the acetyl group, which is included to facilitate purification of the complex using silica gel column chromatography. Complex **1** was obtained by precipitation from the reaction mixture upon completion of the reaction. Complex **2**, which bears solubilizing peripheral *tert*-butyl groups, required column chromatography for purification. In the synthesis of the axially unsymmetrically substituted complexes, **3** and **4**, both ligands were added at the same time and each reaction resulted in a mixture of three complexes; the bis-*S*-(pyridine-4-ylmethyl)ethanethioate and bis-4-*tert*-butylpyridine complexes, and the desired axially unsymmetrical complexes, which were separated using column chromatography. Thus, yields of the unsymmetrical complexes were relatively low. However, given that the expected statistical ratio of the three complexes is 1:1:2, respectively, the theoretical yields of **3** and **4** are half those of **1** and **2**. On this basis, the yields of **3** and **4** are comparable to those of **1** and **2**.

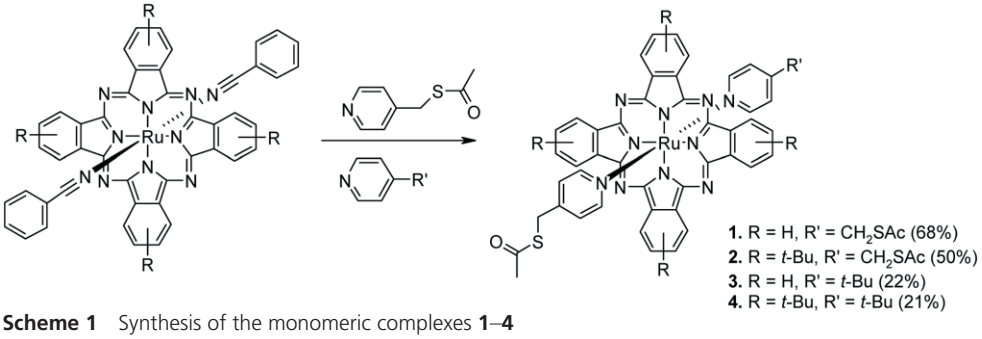

Scheme 1 Synthesis of the monomeric complexes **1**–**4**

The ^{1}H NMR spectra of complexes **1**–**4** are typical of axially substituted PcRu and tetra-*tert*-butyl Pc complexes [5]. The macrocyclic protons of **1** and **3** appear as two

AA′BB′ patterns at low field. Tetra-substitution of **2** and **4** leads to three macrocyclic resonances which are broadened by the mixture of four positional isomers [5]. Pair-wise comparison of the axial ligand resonances of **1** and **2**, and **3** and **4**, shows that peripheral ring substitution with *t*-butyl groups has little effect on the extent of the shielding of the axial ligands.

The complexes **1**–**4** have electronic spectra characteristic of PcRu complexes [5]. They display intense Soret bands with maxima at 314–316 nm with an accompanying low-energy shoulder, and Q-bands with maxima at 624–633 nm and accompanying high-energy shoulders. The Soret bands remain at relatively constant energies across the series of complexes while the energies of the Q-band maxima vary somewhat between the complexes. This is illustrated in the UV–vis spectra of complexes **1** and **2** shown in Fig. 2. Bathochromic shifts of the Q-band of ~160 cm^{-1} are caused by the peripheral *tert*-butyl groups.

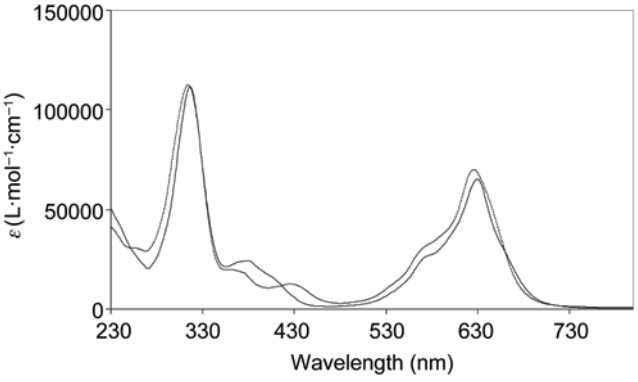

Figure 2 UV–vis spectra of 1 and 2 in dichloromethane solution

1.2 Thin film experiments

Thin films of **1**–**4** were prepared by immersion of gold substrates in dichloromethane solutions containing the complex and tetrabutylammonium hydroxide. The latter was included to hydrolyse the acetyl protecting groups and facilitate binding of the molecule to the surface via the sulfur atom. The films were then thoroughly rinsed with dichloromethane and dried under a stream of nitrogen gas. STM images were obtained for complexes **1** and **4**.

STM images of a thin film of **1** (Fig. 3) reveal an ordered film with the molecules arranged in rows. Individual Pc units are evident in the image shown in Fig. 3(b) and confirm that the molecules are in an "umbrella-type" [17] orientation with the macrocyclic ring coplanar with the surface. Comparison of STM images of **1** with those reported for four-coordinate iron, cobalt, and copper Pc monolayers on gold [18–20] reveals that the coverage is significantly lower for the new ruthenium complex. A surface density of 1.3×10^{13} molecules/cm^2 for **1** was determined by counting the number of molecules in the STM images and dividing by the image area. Coverages of ~4×10^{13} – 5×10^{13} molecules/cm^2 were obtained similarly by inspection of the reported STM images of the four-coordinate iron, cobalt, and copper Pc monolayers on gold [18–20]. While the STM images of **1** reveal row-like formations, the images of the four coordinate metallophthalocyanine complexes on gold show almost quadratic unit cells, which accounts for the difference in coverage. This indicates that binding via the axial ligands of **1** to the gold surface affects surface coverage compared to the four coordinate Pc complexes where the macrocycle adheres directly

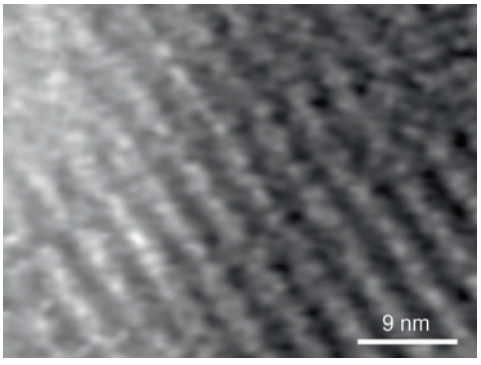

(a)

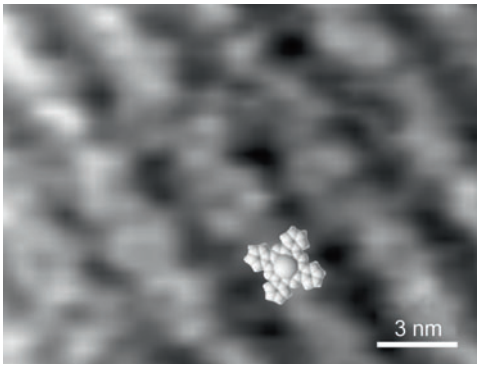

(b)

Figure 3 STM images of a thin film of **1** on a Au(111) surface. Panel (b) shows a magnified image and contains a model of the PcRu unit overlaid on the STM image. Image 2(b) is contrast-enhanced by applying a correlation averaging procedure and a low-pass filter

to the surface. A comparison with four-coordinate PcRu is not possible as this complex does not exist in monomeric form but rather as a dimer, $(PcRu)_2$ [5]. However, Huc et al. [7] reported a coverage of ~5 × 10^{13} molecules/cm^2 estimated by UV-visible spectroscopy for a six-coordinate PcRu complex bound to gold by an axial ligand exchange reaction with a pyridine-modified substrate.

In contrast to **1**, STM images of thin films of **4** (see Fig. 4) reveal a lack of molecular ordering. Features in the STM images corresponding in size to individual molecules are visible but neither the row-type structures seen in **1** nor the regular patterns seen in the four-coordinate metal Pc complexes are observed. A factor that may influence the surface ordering involves the inclusion of the four peripheral tertiary butyl groups that may lead to four possible positional isomers of the $(t\text{-Bu})_4$Pc ring. These isomers could not be separated and thus the potential for ordering of these complexes is somewhat limited.

Although STM can provide useful data about coverage and ordering over small areas, extrapolating the data to the whole surface may not be valid as the film may not be uniform throughout. We therefore quantitatively determined the total number of surface absorbed molecules using a solution ICP-MS technique [21]. Films were completely dissolved in aqua regia, and the amount of ruthenium in the resulting solution was quantified using ICP-MS. Surface density was then calculated by dividing the total amount of ruthenium (there is one ruthenium atom per molecule) by the area of the gold substrate. The results are shown in Table 1.

The ICP-MS data indicate that thin films of **1** have surface densities of ~5.7 × 10^{13} molecules/cm^2, which is significantly larger that the value indicated by STM. The difference between the ICP-MS and STM derived densities indicates that the thin films contain regions of molecules not identified by STM, which may be in the form of aggregates or multi-layers. The ICP-MS derived surface densities for thin films of **3** are similar to those observed in the STM images of **1** suggesting that thin films of **3** are aggregate- and multilayer-free and are likely to be at monolayer coverage. The difference in coverage between **1** and **3** may be a function of the second, unbound axial ligand. In case of **1**, the free axial thiolate group of a surface-bound molecule may couple to other molecules of deprotected **1** in solution via disulfide (–S–S–) linkages to form multilayers. In the case of **2**, this is not possible as the unbound axial ligand bears an unreactive *tert*-butyl group.

Complexes with peripheral *tert*-butyl groups, **2** and **4**, produce films with similar surface densities to each other (Table 1) which, as expected, are lower than those of **1** and **3**. From molecular modeling [22], we estimate the area occupied by a single molecule of $[\{(t\text{-Bu}_4)\text{Pc}\}\text{Ru}(4\text{-py}CH_2SAc)_2]$ on the surface to be ~2.0 × 2.0 nm^2 and so coverages of up to 2.5 × 10^{13} molecules/cm^2 may be expected for close packed monolayers of $[\{(t\text{-Bu}_4)\text{Pc}\}\text{Ru}(4\text{-py}CH_2SAc)_2]$. The measured surface coverage therefore indicates that the molecules to do not form close packed layers.

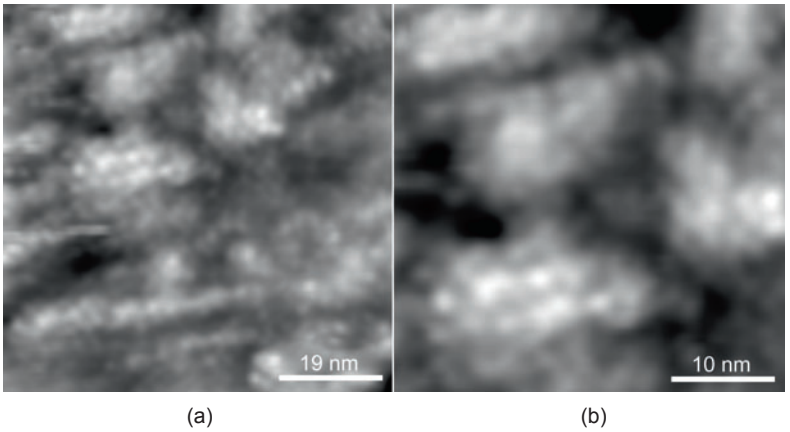

Figure 4 STM images of a thin film of **4** on Au(111). Panel (b) shows a magnified image of the central region of the image shown in (a)

Table 1 ICP-MS and LA-ICP-MS data for thin films of **1**–**4**.

Complex	Molecules (×10^{13}cm^2)[a]	^{101}Ru/^{97}Mo Intensity[b]
1	5.73 ± 0.06	0.706 ± 0.072
2	0.49 ± 0.02	0.358 ± 0.026
3	1.71 ± 0.01	0.148 ± 0.015
4	0.36 ± 0.11	0.0881 ± 0.0042

[a] From solution ICP-MS experiments; [b] By LA-ICP-MS.

This is consistent with the STM images of a thin film of **4** where no ordering was apparent.

We found that laser ablation ICP-MS (LA-ICP-MS) experiments provided valuable information about thin films of the PcRu complexes. LA-ICP-MS analysis of the thin films involved ablating time-resolved lines across the substrate. During the ablation process (see Fig. 5(a)) the adsorbed PcRu molecules were vaporized along with the underlying gold. The ablated material was swept by argon carrier gas to the ICP-MS where the intensities of the ^{101}Ru and ^{197}Au signals were measured together with the ^{97}Mo signal from a standard molybdenum-impregnated glass standard reference material (NIST 612 SRM). The more abundant ^{102}Ru and ^{104}Ru isotopes were found to be unsuitable probes as trace amounts of palladium in the gold substrate resulted in an isobaric interference. We note that trace amounts of silver were also detected in the gold substrates. However, isotopes exist for all transition metal elements that are free from interference from palladium and silver isotopes. Thus, in general, the utility of the technique is not compromised by the presence of these two contaminants. Importantly, the intensity of the ^{101}Ru signal is proportional to the density of ruthenium atoms on the gold surface, and therefore can provide information about the coverage of molecules on the surface. The technique required no additional sample preparation, there were no solvent or matrix interferences, and information about the spatial distribution of the probed elements was obtained.

Data for a single scan of thin films of **2** are shown in Fig. 5(b), where the intensity of the ^{101}Ru and ^{197}Au signals are plotted as a function of distance traversed by the laser across the substrate surface. The signal generated from ^{197}Au is uniform across the ablated region, reflecting the uniform thickness of the gold substrate. The intensity of the ^{101}Ru signal is also essentially even across the ablated region, indicating that the film is uniform. The signal intensity generated by the thin film is in the order of 2000 counts per second, which is well within the sensitivity range of the instrument. In general, relative standard deviations (RSDs) of 15%–25% were obtained for ^{197}Au, ^{99}Ru, ^{100}Ru, and ^{101}Ru. The less abundant isotopes, ^{96}Ru and ^{98}Ru, showed greater variance in signal, most likely due to the lower sensitivity for these ions. Analysis of samples that were not washed with solvent after immersion in the complex solution revealed that while the gold signal remained constant across the length of the sample, the ^{101}Ru signal varied significantly with distance indicating inhomogeneity within the film, attributed to aggregates of PcRu molecules on the surface. This highlights the importance of thorough rinsing of specimens in thin film formation experiments.

A control experiment using [{(t-Bu)$_4$Pc}Ru(4-pyNO$_2$)$_2$] [23], a complex with no surface binding groups, showed that an insignificant amount of the

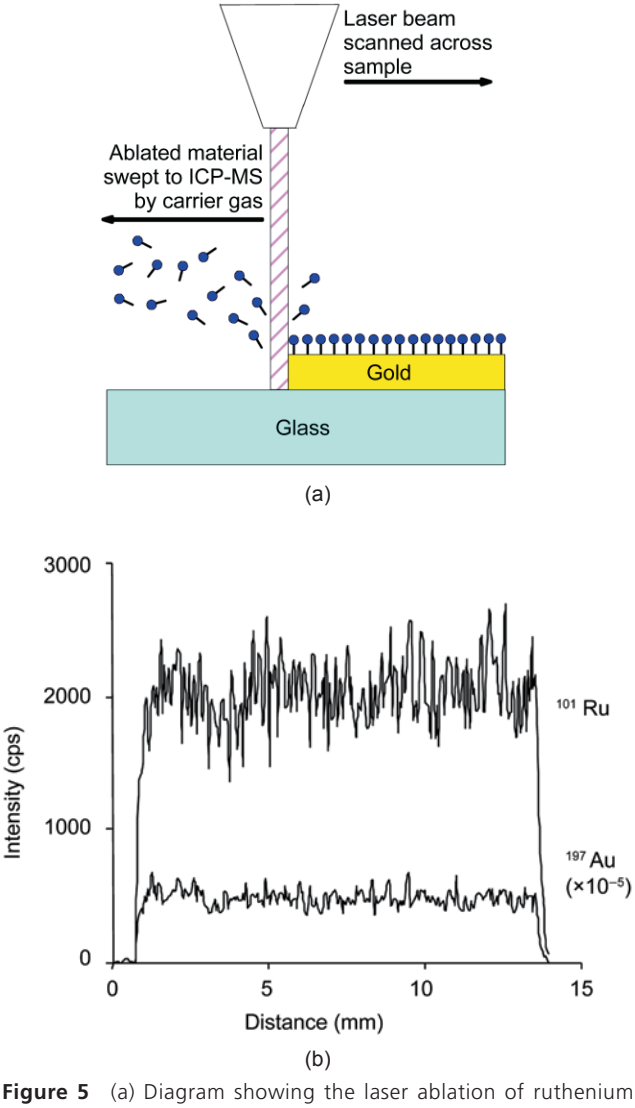

Figure 5 (a) Diagram showing the laser ablation of ruthenium phthalocyanine molecules together with the underlying gold layer; (b) LA-ICP-MS signals of ^{101}Ru and ^{197}Au generated from a single scan of a thin film of the ruthenium phthalocyanine complex on gold

compound remained on the surface after washing; an intensity ratio 15 times less than the corresponding sulfur-containing complex was recorded.

As mentioned above, the ^{101}Ru signal intensity is proportional to the density of PcRu molecules in the thin film. Surface densities were not determined quantitatively using the LA-ICP-MS method but the data provide valuable information on the relative densities of the films. The data were normalized to the molybdenum-impregnated glass standard to account for any signal intensity variability between measurements. The LA-ICP-MS results for **1**–**4** are presented in Table 1 as the intensity ratio of the ^{101}Ru signal to the standard ^{97}Mo signal.

Pair-wise comparison of **1** and **2**, and **3** and **4**, shows that peripheral substitution of the Pc ring reduced the intensity ratios recorded for each film. This trend is in good agreement with the ICP-MS surface density data. The highest intensity ratio was recorded for films of **1**, which had the highest surface density. Films of **4** gave the lowest intensity ratio in the series and had the lowest surface density. Films of **2** were found by ICP-MS to have similar surface densities to those of **4** and it was expected they would have similar intensity ratios. Thin films of **2**, however, had a somewhat higher intensity ratio than that of **4**. The presence of aggregates in the ablated region is not a likely cause as aggregates are readily detected in the LA-ICP-MS line scans as a local increase in signal intensity beyond that of the RSD. The results presented above clearly demonstrate the usefulness of ICP-MS and LA-ICP-MS in the analysis of the ruthenium-containing thin films.

The LA-ICP-MS technique was then applied to gain important insights into the adsorption of **2** on gold. Figure 6 shows the intensity ratios of the ^{101}Ru isotope versus that of a ^{97}Mo standard for films prepared by immersion in the complex solution for periods of 1 min up to 23 h. Interestingly, the films reached a maximum coverage within only one minute of immersion of the substrate in the complex solution; additional immersion time did not increase surface density. Previous studies on the kinetics of thiol-based monolayer formation on gold have reported adsorption times generally on the order of minutes [24]. A two-step adsorption process observed

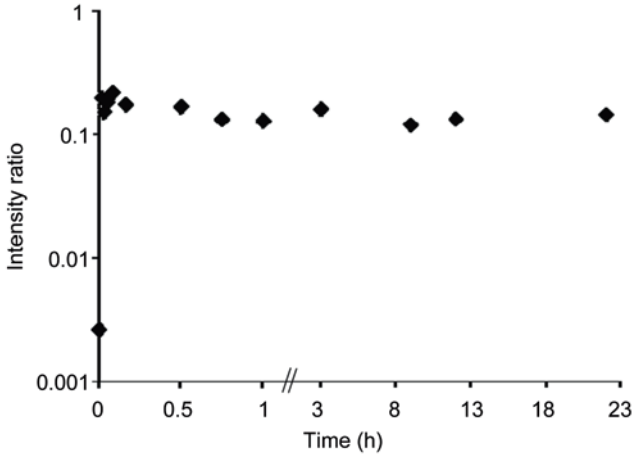

Figure 6 Intensity ratio (^{101}Ru:^{97}Mo) vs. immersion time of gold surfaces in a [{(*t*-Bu)$_4$Pc}Ru(4-pyCH$_2$SAc)$_2$] / TBAOH solution

for alkanethiols on gold using ellipsometry [25], IR [26, 27], and X-ray spectroscopies [28] involves an initial rapid adsorption of molecules onto the gold surface (within one minute) resulting in an imperfect monolayer. A second, slower process was proposed whereupon the monolayer undergoes self-organization with little or no change in the total number of thiol molecules adhered to the gold surface. The data collected in the current work are consistent with this timeframe for initial adsorption of the hitherto unreported complex.

2. Conclusions

Four new ruthenium phthalocyanine complexes have been prepared bearing axial ligands with thioacetate groups that facilitate thin film formation on gold surfaces. STM images of a thin film of complex **1**, which bears no peripheral substituents, revealed an ordered film while images obtained for complex **4**, which bears four peripheral *t*-butyl groups and exists as a mixture of positional isomers revealed no apparent ordering of the molecules. The surface coverage data obtained by solution ICP-MS experiments were consistent with the STM experiments and revealed that more molecules of the unsubstituted complexes **1** and **3** occupied the substrate surface than molecules of the substituted complexes **2** and **4**. From these experiments, it is clear that peripheral and axial ligand substituents on the complexes have a significant effect on their surface coverage.

The LA-ICP-MS technique described here for the first time is ideally suited to the analysis of these thin films due to the sensitive nature of the technique as well as the lack of interferences with the Ru isotope analyzed. The method is rapid and reliable and provides information about films across macro-sized areas. We have used the technique to study the adsorption of the new complex on gold surfaces and found that maximum coverage occurred within one minute of substrate immersion. We envisage that this technique may find widespread application in the analysis of metal-containing thin films.

3. Experimental

3.1 General

^{1}H NMR spectra were recorded using a BVT 3000 Bruker Spectrospin instrument operating at 300.13 MHz. Spectra are referenced internally to residual protic solvent ($CHCl_3$, δ 7.26). UV–vis spectra were recorded using an Agilent 8453 UV–vis spectrophotometer with dichloromethane used as solvent. Electrospray ionization mass spectra (ESI-MS) were recorded using a Perkin-Elmer SCIEX API300 Triple Quadrupole Mass Spectrometer. The general conditions were: ion spray voltage = 5000 V, drying gas temperature = 50 °C, orifice voltage = 30 V, ring voltage = 340 V, and injection via syringe pump. Spectra were averaged over 10 scans. Elemental microanalyses were performed by the Microanalytical Service at the Australian National University.

[PcRu(PhCN)$_2$] [29], *S*-(pyridine-4-ylmethyl)ethanethioate (4-pyCH_2SAc) [30], and [{(*t*-Bu)$_4$Pc}Ru(PhCN)$_2$] [23] were prepared by literature procedures. The following were purchased commercially and used as received; pyrazine (Aldrich), 4-*tert*-butylpyridine (Aldrich), tetrabutylammonium hydroxide (Aldrich), nitric acid Baseline grade (Seastar), hydrochloric acid Baseline grade (Seastar), gold 99.99% (AGR Matthey).

3.2 Synthesis

3.2.1 *Preparation of [PcRu(4-pyCH_2SAc)$_2$] (**1**)*

[PcRu(PhCN)$_2$] (70 mg, 0.09 mmol) and 4-pyCH_2SAc (43 mg, 0.26 mmol) were dissolved in deoxygenated dichloromethane (30 mL). The resulting solution was heated at reflux for 3 h under a nitrogen atmosphere then allowed to cool. The volume of the solution was reduced to ~10 mL by rotary evaporation, filtered, and then methanol (30 mL) was added to the filtrate. The resulting cloudy solution was allowed to stand overnight and then filtered, affording 55 mg (68%) of a dark blue powder. ^{1}H NMR (δ, 300 MHz, $CDCl_3$): 9.12 (*m*, 8 H, Pc), 7.88 (*m*, 8H, Pc), 5.13 (*d*, J_{HH} = 6.9 Hz, 4H, py), 2.81 (*s*, 4H, CH_2), 2.34 (*d*, J_{HH} = 6.9 Hz, 4H, py), 1.89 (*s*, 6H, CH_3). UV–vis (λ_{max}, nm [ε, 10^3 mol·L^{-1}·cm^{-1}]): 624 [64], 569sh, 379sh, 314 [99]. MS (*m*/*z*) 949 ([M + H]$^+$, 100). Anal. Calcd for $C_{48}H_{34}N_{10}O_2RuS_2$: C 60.81, H 3.61, N 14.77. Found: C 59.42, H 3.73, N 15.09.

3.2.2 *[{(t-Bu)$_4$Pc}Ru(4-pyCH_2SAc)$_2$] (**2**)*

[{(*t*-Bu)$_4$Pc}Ru(PhCN)$_2$] (150 mg, 0.14 mmol) and 4-pyCH_2SAc (72 mg, 0.43 mmol) were dissolved in deoxygenated dichloromethane (30 mL). The solution was heated at reflux for 3 h under a nitrogen atmosphere. The solvent was removed *in vacuo*, and the crude product purified by silica column chromatography eluting with dichloromethane: hexane (4:1). After evaporation of the solvent, 85 mg (50%) of blue powder was collected. ^{1}H NMR (δ, 300 MHz, $CDCl_3$): 9.17 (*m*, 4H, Pc), 9.05 (*m*, 4H, Pc), 7.94 (*m*, 4H, Pc), 5.11 (*d*, J_{HH} = 6.6 Hz, 4H, py), 2.80 (*s*, 4H, CH_2), 2.35 (*d*, J_{HH} = 6.9 Hz, 4H, py), 1.89 (*s*, 6H, CH_3), 1.73 (*m*, 36H, *t*-Bu). UV–vis (λ_{max}, nm [ε, 10^3 mol·L^{-1} ·cm^{-1}]): 629 [65], 579sh, 378sh, 316 [111]. MS (*m*/*z*) 1173 ([M + H]$^+$, 100). Anal. Calcd for $C_{64}H_{66}N_{10}O_2RuS_2$: C 65.56, H 5.67, N 11.95. Found: C 65.97, H 6.26, N 12.14.

3.2.3 *[PcRu(4-t-Bupy)(4-pyCH_2SAc)] (**3**) and [{(t-Bu)$_4$Pc}Ru(4-t-Bupy)(4-pyCH_2SAc)] (**4**)*

The same procedure was used to prepare complexes **3** and **4**. The preparation of [{(*t*-Bu)$_4$Pc}Ru(4-*t*-Bupy)(4-pyCH_2SAc)] **4** is given as an example. [{(*t*-Bu)$_4$Pc}Ru(PhCN)$_2$] (300 mg, 0.29 mmol), 4-pyCH_2SAc (96 mg, 0.57 mmol) and 4-*t*-Bupy (78 mg, 0.57 mmol) were dissolved in deoxygenated dichloromethane (60 mL). The solution was heated at reflux for 3 h under a nitrogen atmosphere. The

solvent was removed *in vacuo*, and the crude product purified by silica column chromatography eluting with dichloromethane:hexane (3:1). The second band to elute was collected, affording 68 mg (21%) of blue powder after evaporation of the solvent. ^{1}H NMR (δ , 300 MHz, $CDCl_3$): 9.17 (*m*, 4H, Pc), 9.05 (*m*, 4H, Pc), 7.94 (*m*, 4H, Pc), 5.16 (*d*, J_{HH} = 6.9 Hz, 2H, py), 5.12 (*d*, J_{HH} = 6.6 Hz, 2H, py), 2.81 (*s*, 2H, CH_2), 2.40 (*d*, J_{HH} = 6.9 Hz, 2H, py), 2.37 (*d*, J_{HH} = 6.9 Hz, 2H, py), 1.90 (*s*, 3H, CH_3), 1.74 (*m*, 36H, *t*-Bu), 0.31 (*s*, 9H, *t*-Bu). UV–vis (λ_{max}, nm [ε , 10^3 mol·L^{-1}·cm^{-1}]): 629 [58], 576sh, 376sh, 316 [98]. MS (*m*/*z*) 1141 ([M + H]$^+$, 100). Anal. Calcd for $C_{65}H_{70}N_{10}ORuS$: C 68.46, H 6.19, N 12.28. Found: C 68.54, H 5.78, N 11.60.

3.2.4 *[PcRu(4-t-Bupy)(4-pyCH$_2$SAc)] (3)*

Blue powder (yield 22%). ^{1}H NMR (δ , 300 MHz, $CDCl_3$): 9.13 (*m*, 8H, Pc), 7.88 (*m*, 8H, Pc), 5.18 (*d*, J_{HH} = 7.2 Hz, 2H, py), 5.14 (*d*, J_{HH} = 6.9 Hz, 2H, py), 2.82 (*s*, 2H, CH_2), 2.38 (*d*, J_{HH} = 6.9 Hz, 2H, py), 2.34 (*d*, J_{HH} = 6.9 Hz, 2H, py), 1.90 (*s*, 3H, CH_3), 0.31 (*s*, 9H, *t*-Bu). UV–vis (λ_{max}, nm [ε , 10^3 mol·L^{-1}·cm^{-1}]): 624 [66], 571sh, 375sh, 315 [97]. MS (*m*/*z*) 916 ([M]$^+$, 100). Anal. Calcd for $C_{49}H_{38}N_{10}ORuS$: C 64.25, H 4.18, N 15.29. Found: C 64.72, H 4.43, N 16.96.

3.3 Surface experiments

3.3.1 *Substrates and assembly*

Glass slides (10 mm × 10 mm) were washed by sonicating sequentially in acetone, water (Milli-Q), buffered hydrofluoric acid [31], and then water. The slides were then coated with gold by vacuum deposition using a Denton Turbo deposition system. A 300 nm layer of gold was deposited on the glass substrates at an approximate rate of 2–3 Å/s. Scintillation vials were washed overnight in 30% HNO_3 before being rinsed with water (Milli-Q) and then oven dried. 1 mmol/L dichloromethane solutions of the complexes were prepared in the cleaned vials. Tetrabutylammonium hydroxide (3 mmol/L) was added and the solution sonicated for 5 min before the gold substrate was placed within the vial. The vials were then stored overnight in a nitrogen atmosphere and shielded from light. For surface density vs. immersion time experiments, the gold slides were immersed in a solution of **2** for 1, 2, 3, 5, 10, 15, 30, and 45 min, and 1, 3, 6, 9, 12, and 22 h. When removed, the gold substrates were immediately rinsed with dichloromethane, then sonicated in dichloromethane for 5 min. The thin films were dried under a stream of nitrogen gas and analysed by ICP-MS promptly.

3.3.2 *Scanning Tunneling Microscopy*

A Digital Instruments Multimode Nanoscope III was used for scanning tunneling microscopy (STM) and for these experiments Au(111) films on mica were used (Molecular Imaging, USA) and flame annealed before use. The STM tip was prepared from Pt/Ir (90:10) wire cut under ambient conditions. All images were acquired in a constant-current mode. Typical imaging conditions are bias voltages of –0.1 to –0.5 V and a tunneling current of 100–500 pA. Images shown are raw data unless stated otherwise. Images were manipulated with the Scanning Probe Image Processor (SPIP) software. Contrast-enhanced images were obtained by applying a correlation averaging procedure to analyze repeat molecular units and by applying a low-pass filter.

3.3.3 *LA-ICP-MS*

A New Wave (Fremont, CA, USA) UP213 laser ablation unit, coupled to an Agilent Technologies 7500ce Series ICP-MS was used to analyze the thin films. The laser system was a Nd:YAG laser operating at the fifth harmonic frequency (213 nm) with a repetition frequency of 10 Hz and beam diameter of 55 μm. The laser was operated at 25% power density giving ~0.11 J/cm^2 and scanned across the substrate to a speed of 70 μm/s. The substrates were secured on a glass slide using doubled sided adhesive tape and mounted on an *x*–*y*–*z* translation stage, which could be manipulated using a computer and monitored by CCD camera. Standard reference material, NIST 612, was also placed in the chamber and ablated *prior to* the substrate to determine any instrumental changes that may occur between sample runs. The ablated material was transported to the ICP-MS by argon carrier gas. Gold (^{197}Au) and all ruthenium isotopes (^{96,98,99,100,101,102,104}Ru) were monitored by the ICP-MS (Rf Power 1300 W, carrier gas flow 1.2 L/min, plasma gas flow 15 L/min, dwell time 100 ms, scan mode:

peak hopping).

Film uniformity was assessed using the RSD calculated from the LA-ICP-MS signal generated from ablation across the length of the substrate.

3.3.4 *Solution ICP-MS*

The area of the thin films was carefully measured and the specimens were then placed in PTFE screw-cap vials. 3 mL of 20% Baseline grade HNO_3 and 0.5 mL of 37% Baseline grade HCl were added to each sample. Samples were allowed to digest for 1 h, followed by sonication for 5 min. The digests were quantitatively transferred to polypropylene vials and diluted to a known mass using 1% HNO_3/HCl. ICP-MS analysis was performed on an Agilent Technologies 7500ce instrument fitted with a "cs" lens system for improved sensitivity. A five-point calibration curve for ^{99,100,101,102}Ru was constructed with a range of 0.1 to 10 μg/kg. Correlation coefficients for each isotope were 1.000 with sub ng/kg detection limits.

Acknowledgements

This work was supported by the Australian Research Council (DP0984354). We thank Dr N. Lucas for Spartan molecular modeling calculations.

References

[1] Nakamura, T. Electrochemical biosensors in nonaqueous solutions and their applications. *Anal. Sci.* **2007**, *23*, 253–259.

[2] Mathiyarasu, J.; Pathak, S. S.; Yegnaraman, V. Review on corrosion prevention of copper using ultrathin organic monolayers. *Corros. Rev.* **2006**, *24*, 307–321.

[3] Smith, R. K.; Lewis, P. A.; Weiss, P. S. Patterning self-assembled monolayers. *Prog. Surf. Sci.* **2004**, *75*, 1–68.

[4] Love, J. C.; Estroff, L. A.; Kriebel, J. K.; Nuzzo, R. G.; Whitesides, G. M. Self-assembled monolayers of thiolates on metals as a form of nanotechnology. *Chem. Rev.* **2005**, *105*, 1103–1169.

[5] Rawling, T.; McDonagh, A. M. Ruthenium phthalocyanine and naphthalocyanine complexes: Synthesis, properties and applications. *Coord. Chem. Rev.* **2007**, *251*, 1128–1157.

[6] Lucas, N. T.; Zareie, H. M.; McDonagh, A. M. Self-organization of a discotic coordination complex bearing orthogonal discotic ligands. *ACS Nano* **2007**, *1*, 348–354.

[7] Huc, V.; Armand, F.; Bourgoin, J. P.; Palacin, S. Covalent anchoring of phthalocyanines on silicon dioxide surfaces: Building up mono- and multilayers. *Langmuir* **2001**, *17*, 1928–1935.

[8] Huc, V.; Bourgoin, J. -P.; Bureau, C.; Valin, F.; Zalczer, G.; Palacin, S. Self-assembled mono- and multilayers on gold from 1,4-diisocyanobenzene and ruthenium phthalocyanine. *J. Phys. Chem. B* **1999**, *103*, 10489–10495.

[9] Huc, V.; Saveyroux, M.; Bourgoin, J. -P.; Valin, F.; Zalczer, G.; Albouy, P. -A.; Palacin, S. Grafting ruthenium phthalocyanine on gold and silica: Using apical ligands as linker. *Langmuir* **2000**, *16*, 1770–1776.

[10] Li, X.; Xu, W.; Wang, X.; Jia, H.; Zhao, B.; Li, B.; Ozaki, Y. Ultraviolet–visible and surface-enhanced Raman scattering spectroscopy studies on self-assembled films of ruthenium phthalocyanine on organic monolayer-modified silver substrates. *Thin Solid Films* **2004**, *457*, 372–380.

[11] Lei, S.; DeFeyter, S. STM, STS and bias-dependent imaging on organic monolayers at the solid-liquid interface. *Top. Curr. Chem.* **2008**, *285*, 269–312.

[12] Vericat, C.; Vela, M. E.; Benitez, G. A.; Gago, J. A. M.; Torrelles, X.; Salvarezza, R. C. Surface characterization of sulfur and alkanethiol self-assembled monolayers on Au(111). *J. Phys.: Condens. Matter* **2006**, *18*, R867–R900.

[13] Russo, R. E.; Mao, X.; Liu, H.; Gonzalez, J.; Mao, S. S. Laser ablation in analytical chemistry—A review. *Talanta* **2002**, *57*, 425–451.

[14] Mrksich, M. Mass spectrometry of self-assembled monolayers: A new tool for molecular surface science. *ACS Nano* **2008**, *2*, 7–18.

[15] Narine, S. S.; Hughes, R.; Slavin, A. J. The use of inductively coupled plasma mass spectrometry to provide an absolute measurement of surface coverage, and comparison with the quartz crystal microbalance. *Appl. Surf. Sci.* **1999**, *137*, 204–206.

[16] Pritzkow, W.; Vogl, J.; Berger, A.; Ecker, K.; Groetzschel, R.; Klingbeil, P.; Persson, L.; Riebe, G.; Waetjen, U. Contribution of ICP-IDMS to the certification of antimony implanted in a silicon wafer—Comparison with RBS and INAA results. *Fresenius J. Anal. Chem.* **2001**, *371*, 867–

873.

[17] Li, Z.; Lieberman, M.; Hill, W. XPS and SERS study of silicon phthalocyanine monolayers: Umbrella vs. octopus design strategies for formation of oriented SAMs. *Langmuir* **2001**, *17*, 4887–4894.

[18] Cheng, Z. H.; Gao, L.; Deng, Z. T.; Jiang, N.; Liu, Q.; Shi, D. X.; Du, S. X.; Guo, H. M.; Gao, H. J. Adsorption behavior of iron phthalocyanine on Au(111) surface at submonolayer coverage. *J. Phys. Chem. C* **2007**, *111*, 9240–9244.

[19] Hipps, K. W.; Lu, X.; Wang, X. D.; Mazur, U. Metal d-orbital occupation-dependent images in the scanning tunneling microscopy of metal phthalocyanines. *J. Phys. Chem.* **1996**, *100*, 11207–11210.

[20] Yoshimoto, S. Molecular assemblies of functional molecules on gold electrode surfaces studied by electrochemical scanning tunneling microscopy: Relationship between function and adlayer structures. *Bull. Chem. Soc. Jpn.* **2006**, *79*, 1167–1190.

[21] Zheng, Z.; Yang, M.; Liu, Y.; Zhang, B. Direct patterning of negative nanostructures on self-assembled monolayers of 16-mercaptohexadecanoic acid on Au(111) substrate via dip-pen nanolithography. *Nanotechnology* **2006**, *17*, 5378–5386.

[22] Equilibrium geometry optimization was achieved using the molecular mechanics method (MMFF94 force fields). Spartan'04, Wavefunction Inc., 2004, Irvine, CA, USA.

[23] Rawling, T.; Xiao, H.; Lee, S. -T.; Colbran, S. B.; McDonagh, A. M. Optical and redox properties of ruthenium phthalocyanine complexes tuned with axial ligand substituents. *Inorg. Chem.* **2007**, *46*, 2805–2813.

[24] Schreiber, F. Structure and growth of self-assembling monolayers. *Prog. Surf. Sci.* **2000**, *65*, 151–256.

[25] Bain, C. D.; Troughton, E. B.; Tao, Y. T.; Evall, J.; Whitesides, G. M.; Nuzzo, R. G. Formation of monolayer films by the spontaneous assembly of organic thiols from solution onto gold. *J. Am. Chem. Soc.* **1989**, *111*, 321–335.

[26] Bensebaa, F.; Voicu, R.; Huron, L.; Ellis, T. H.; Kruus, E. Kinetics of formation of long-chain *n*-alkanethiolate monolayers on polycrystalline gold. *Langmuir* **1997**, *13*, 5335–5340.

[27] Truong, K. D.; Rowntree, P. A. Kinetics of the formation of butanethiol monolayers on gold substrates, as studied by infrared spectroscopy. *Prog. Surf. Sci.* **1995**, *50*, 207–216.

[28] Haehner, G.; Woell, C.; Buck, M.; Grunze, M. Investigation of intermediate steps in the self-assembly of *n*-alkanethiols on gold surfaces by soft X-ray spectroscopy. *Langmuir* **1993**, *9*, 1955–1958.

[29] Bossard, G. E.; Abrams, M. J.; Darkes, M. C.; Vollano, J. F.; Brooks, R. C. Convenient synthesis of water soluble, isomerically pure ruthenium phthalocyanine complexes. *Inorg. Chem.* **1995**, *34*, 1524–1527.

[30] Balkovec, J. M.; Szymonifka, M. J.; Heck, J. V.; Ratcliffe, R. W. Basic carbapenem analogs: Synthesis and *in vitro* activity of 1b-methyl-2-(pyridylmethylthio)-carbapenems. *J. Antibiot.* **1991**, *44*, 1172–1177.

[31] Xu, X.; Cortie, M. B.; Stevens, M. Effect of glass pre-treatment on the nucleation of semi-transparent gold coatings. *Mater. Chem. Phys.* **2005**, *94*, 266–274.